American Mineralogist, Volume 93, pages 39–47, 2008

Comparative Raman spectroscopic study on ilmenite-type $MgSiO_3$ (akimotoite), $MgGeO_3$, and $MgTiO_3$ (geikielite) at high temperatures and high pressures

Taku Okada,* Toshiharu Narita, Takaya Nagai,† and Takamitsu Yamanaka

Department of Earth and Space Science, Graduate School of Science, Osaka University, 1-1 Machikaneyama, Toyonaka, Osaka 560-0043, Japan

Abstract

The Raman spectra of $MgXO_3$-ilmenites (X = Si, Ge, Ti) were recorded up to 773 K at ambient pressure and up to 20–30 GPa at room temperature. Temperature and pressure dependence of the force constant of X-O stretching bands revealed that the expansion and compression behavior of XO_6 octahedra differed in the three ilmenites. For SiO_6 and GeO_6 octahedra, the shorter Si-O or Ge-O bonds became more lengthened with temperature and more shortened with pressure than did the longer Si-O or Ge-O bonds. In contrast, for TiO_6 octahedra, the longer Ti-O bonds became more lengthened with temperature and more shortened with pressure than did the shorter Ti-O bonds. For SiO_6 and GeO_6 at high temperatures and TiO_6 at high pressures, the cation positions moved in the direction of the **c** axis and tended to approach the center of the octahedra, decreasing the distortion of XO_6. For SiO_6 and GeO_6 at high pressures and TiO_6 at high temperatures, the cations moved away from the center, increasing the distortion of XO_6. One of the anharmonic correction terms on isochoric specific heat was also elucidated. The anharmonic effects were related to the elastic Debye temperature of the three ilmenites.

Keywords: Raman spectroscopy, ilmenite, high temperature, high pressure, crystal structure

Introduction

The $M^{2+}X^{4+}O_3$-ilmenite structure has unique face-shared and edge-shared configurations of MO_6 and XO_6 octahedra (Fig. 1). Cation-cation interactions in the structure affect the physical properties. Ilmenite compounds have a relatively large M cation (M: Mg, Fe, Mn, Co, Zn) and a small X cation (X: Si, Ge, Sn, Ti). However, compounds with a large ion radius ratio (R_M/R_X), such as $CaTiO_3$ and $BaTiO_3$, do not form ilmenite-type structures but have the perovskite structure at ambient pressure. Many ilmenite-structured compound transform into a perovskite structure at high pressure because oxygen is more compressible than the cations and thus the $(R_M\text{-}R_O)/(R_X\text{-}R_O)$ ratio increases with pressure. Pressure-temperature regions of stability vary systematically with the cation radius ratios. Ilmenite-type $MgSiO_3$ is one of the high-pressure polymorphs of orthoenstatite, characterized by a relatively low-temperature and narrow-stability field in the 20–24 GPa below the 2300 K range (Sawamoto 1987), and thus is considered a candidate component at 600–700 km depths in subducting slabs. (Mg,Fe)SiO_3-ilmenite was found in the shock vein of meteorite and named akimotoite (Tomioka and Fujino 1997). $MgGeO_3$ shows the same polymorphic transitions as $MgSiO_3$, but its transition pressures are much lower than the corresponding pressures of the $MgSiO_3$ polymorphs (Ross and Navrotsky 1988). $MgTiO_3$-ilmenite (geikielite) is found as an accessory mineral in many igneous and metamorphic rocks (Deer and Zussman 1963) and can be synthesized at ambient pressure (Linton et al. 1999).

$MgSiO_3$ in the ilmenite structure was analyzed by a single-crystal X-ray diffraction (XRD) study under ambient conditions (Horiuchi et al. 1982) and by powder XRD methods at high pressure (Reynard et al. 1996). Molecular dynamic simulations of $MgSiO_3$-ilmenite have been also carried out (Matsui et al. 1987; Karki et al. 2000). Yamanaka et al. (2005) conducted a single-crystal XRD study under high pressures on $MgSiO_3$-, $MgGeO_3$-, and $MgTiO_3$-ilmenites and obtained the pressure dependence of interatomic distances, bond angles, and bulk moduli of their unit cells and octahedral volumes. They reported that the MgO_6 octahedral volume is much more compressive than that of XO_6, and both MgO_6 and XO_6 (X = Si, Ge, Ti) octahedra are most rigid in $MgSiO_3$ of the three ilmenite types. They have showed that the Mg-X interatomic distance becomes more shortened with increasing pressure than do the Mg-Mg and X-X distances.

Pressure provided by the external system, P_{ext}, affects not only the atomic positions (leading the interatomic distances) but also interatomic bonding force, as the following virial equation of state:

$$P_{ext} = \frac{Nk_BT}{V} - \frac{1}{3V}\left\langle \sum_{i=1}^{N}\sum_{j>1}^{N}\left(-\frac{\partial \psi_{ij}}{\partial r_{ij}}\right)\cdot \boldsymbol{r}_{ij}\right\rangle = \frac{Nk_BT}{V} - \frac{1}{3V}\left\langle \sum_{i=1}^{N}\sum_{j>1}^{N} F_{ij}\cdot r_{ij}\right\rangle \quad (1)$$

* Present Address: Institute for Solid State Physics, University of Tokyo, 5-1-5 Kashiwanoha, Kashiwa, Chiba 277-8581, Japan. E-mail: okataku@issp.u-tokyo.ac.jp

† Present Address: Division of Earth and Planetary Science, Graduate School of Science, Hokkaido University, N10 W8, Sapporo, Hokkaido 060-0810, Japan.

0003-004X/08/0001–039$05.00/DOI: 10.2138/am.2008.2490

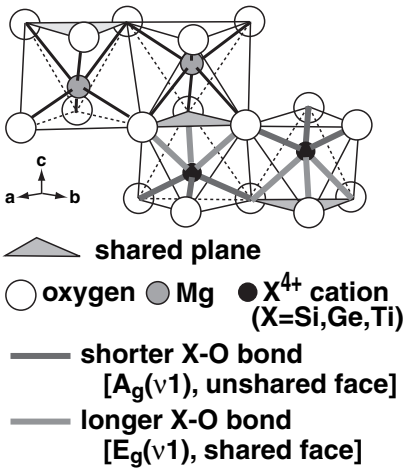

FIGURE 1. Linkage of MgO_6 and XO_6 (X = Si, Ge, Ti) octahedra.

where V is the cell volume, N is the number of particles, k_B is Boltzman constant, Ψ_{ij} is the internal potential between i and j atom, r_{ij} is the interatomic distances, and F_{ij} is the interatomic bonding force which comes out from j to i atom. Raman spectroscopic studies provide information about the vibration of each atom and, thus, a crystal structure can be discussed based on lattice dynamics such as the interatomic bonding force and bonding energy. The spectroscopy is a complementary method to the XRD study. However, to obtain the interatomic bonding force from the Raman frequency, each Raman peak must be assigned to a particular atomic motion. Hofmeister (1993) assigned the Raman peaks of the ilmenite structure, based on ionic substitution. On that basis, we can calculate the force constant from the stretching-band frequency and explain the temperature and pressure dependence of the interatomic force. In this study, we conducted a high-temperature, high-pressure Raman spectroscopic study of $MgSiO_3$-, $MgGeO_3$-, and $MgTiO_3$-ilmenites. We investigated the elastic properties and bonding characteristics of the three ilmenite types at high temperature and high pressure and discuss the chemical compositional dependence of their structural changes.

In the thermodynamic modeling of the high-pressure phase relations, a quasi-harmonic approximation is commonly assumed, and the calculated isochoric specific heat (C_V) tends toward the classical Dulong-Petit limit ($3nR$) at high temperature. However, due to intrinsic anharmonic effects, this approximation fails at high temperature. The anharmonic contribution to the thermodynamic properties of mantle minerals is one of the significant problems at high temperature. One of the anharmonic correction terms can be calculated from the high-temperature, high-pressure Raman spectroscopic data. We present here the anharmonic correction term on the isochoric specific heat. The high-temperature, high-pressure Raman spectra of ilmenite-type $MgSiO_3$ already have been investigated up to 1030 K at ambient pressure and 7 GPa at room temperature (Reynard and Rubie 1996). They concluded that the intrinsic anharmonic corrections to the thermodynamic properties of ilmenite are probably insignificant. Chopelas (1999) calculated C_V from the spectra of $MgSiO_3$-ilmenite at room temperature and found good agreement with the isobaric specific heat (C_P) measured by calorimetry (Ashida et al. 1988). This work also shows that $MgSiO_3$-ilmenite is not anharmonic. We calculate and compare the anharmonic corrections of the three ilmenite types and discuss the origin of the magnitude of the corrections.

EXPERIMENTAL METHODS

A powdered sample of $MgSiO_3$-enstatite was synthesized at ambient pressure and 1800 K for 40 h by solid-state reaction of MgO with SiO_2 using a $MoSi_2$ electric furnace under atmospheric condition. It was used as a starting material and transformed at 22 GPa and 1800 K for 30 min using a 5000 t multi-anvil press installed at Misasa, Okayama University. A semi-sintered MgO octahedron was used as the pressure medium, and a cylindrical Re foil was used as the sample chamber and as the furnace in conjunction with a Ta electrode. The furnace was surrounded by $LaCrO_3$ as a thermal insulator. $MgGeO_3$-ilmenite was synthesized at 6 GPa and 1200 K for 17 h using a cubic-anvil press installed at Osaka University. A pyrophyllite cube was used as the pressure medium and a graphite sleeve was used as heating material. The starting material of the mixture of MgO and GeO_2 was kept in gold tubes sealed at both ends by welding to prevent samples from reducing. $MgTiO_3$-ilmenite was prepared by solid-state reaction of MgO with TiO_2 in a Pt crucible at ambient pressure and 1800 K for 80 h using a $MoSi_2$ electric furnace under atmospheric conditions. To obtain a homogeneous sample, the recovered sample was pulverized and sintered again under the same conditions. The purity and homogeneity of the three samples were confirmed by both microprobe chemical analyses and powder XRD.

The Raman spectra were obtained using the NRS2100-F micro-Raman spectrometer (JASCO, Japan) equipped with a triple-grating monochromator and an Ar ion laser at 514.5 nm. The incident laser beam was focused on the sample using a 20× objective lens (working distance 21.0 mm, SLMPlan, Olympus, Japan). Raman shifts were calibrated with the Ne lamp spectrum as the band calibration standard. High-temperature experiments were performed using a heating stage consisting of a Pt electric-resistance heater with a water-cooled system and a Pyrex glass window. The maximum temperature for the heating stage is 773 K. Temperature was monitored with a chromel-almel thermocouple. The high-temperature Raman spectra of each sample were collected at temperatures of 293, 373, 473, 573, 673, and 773 K at ambient pressure for 300 s exposure time with the operating laser power of 200 mW (for $MgSiO_3$), for 30 s with 70 mW (for $MgGeO_3$), and for 5 s with 80 mW (for $MgTiO_3$). For high-pressure experiments, a diamond-anvil cell was used. The diameter of the culet of the diamond was 350 μm. A 200 μm thick spring steel gasket was preindented to 50 μm, and a sample cavity of 130 μm in diameter was opened using electric discharge machining. The powdered sample was loaded with H_2O as a pressure-transmitting medium and small ruby chips (10 μm in diameter) as pressure markers. H_2O was preferred to an alcohol mixture as the pressure medium because it has no strong Raman bands in the measured region. Pressures were determined from the shift of the ruby fluorescence R_1 line (Mao et al. 1978) excited by the Ar ion laser. High-pressure Raman spectra of each sample were collected at room temperature and up to 31.3 GPa for 300 s exposure time with the operating laser power of 600 mW (for $MgSiO_3$), up to 22.4 GPa for 100 s with 250 mW (for $MgGeO_3$), and up to 31.1 GPa for 100 s with 150 mW (for $MgTiO_3$). We determined the center of each peak by profile fitting using a Lorentzian function with optimizing variables of peak position, peak height, and half width using a commercially available software "ORIGIN."

RESULTS AND DISCUSSION

Temperature and pressure dependence of Raman spectra

The number, type, and symmetry of vibrational modes were inferred from the space group and the placement of the atoms. The ilmenite structure has the $R\bar{3}$ (No. 146) space group. Factor-group analysis (Fateley et al. 1971) gives the symmetry species for the three acoustic modes and 27 optical modes, distributed as follows:

$$\Gamma = 5A_g(R) + 5E_g(R) + 5A_u(1A + 4IR) + 5E_u(1A + 4IR) \quad (2)$$

where R denotes Raman active modes; IR, infrared active modes;

and A, acoustic modes. Hofmeister (1993) measured polarized single-crystal infrared (IR) reflectance spectra of natural ilmenite ($FeTiO_3$). IR and Raman peaks were correlated between these data and previous polycrystalline studies of 14 isostructural compounds by comparing intensity patterns. According to Hofmeister (1993), 10 Raman active bands were assigned: $A_g(\nu_1)$ and $E_g(\nu_1)$ were assigned to X^{4+}-O stretching motions; $A_g(\nu_4)$ and $E_g(\nu_4)$ to translations of the XO_6 octahedra against M^{2+}; $A_g(\nu_5)$ and $E_g(\nu_5)$ to translations of the M^{2+} cation against the oxygen framework; and the remaining bands to O-X^{4+}-O bending. In this study, all 10 Raman active bands of $MgTiO_3$-ilmenite were obtained under ambient conditions (Table 1), the same number as found by White (1974) and Reynard and Guyot (1994). For $MgSiO_3$- and $MgGeO_3$-ilmenites, we obtained only seven and eight bands, respectively (Table 1) although in the previous reports nine (Ross and McMillan 1984; McMillan and Ross 1987; Reynard and Rubie 1996; Chopelas 1999) and 10 (Ross and Navrotsky 1988) Raman bands were observed. These discrepancies could be attributed to our observations in the high-temperature cells through the Pyrex window even under ambient condition. The frequencies of the Raman bands from each ilmenite type under ambient conditions were in agreement with previous determinations within a few wave numbers.

The evolutions of the Raman spectra with temperature and pressure are shown in Figures 2 and 3. With increasing temperature, each band shifted to a lower frequency (Figs. 2a–2c). For $MgGeO_3$ and $MgTiO_3$, all bands that were observed under ambient conditions could be followed up to 773 K. For $MgSiO_3$, the $E_g(\nu_1)$ peak could not be observed at 773 K. Raman frequencies shift linearly with temperature (Table 1; Fig. 4a). During decreasing temperature, no hysteresis was observed. Each band shifts to higher frequency with pressure (Figs. 3a–3c). Frequency shifts with pressure are reported in Table 1 and Figure 4b. For $MgSiO_3$ and $MgGeO_3$, some bands could not be observed at high pressure due to serious decreases in the overall intensity. During decompression, no hysteresis was observed.

Temperature and pressure dependence of the force constant *k*

The force constant, *k*, expressing the interatomic bonding force between atoms, is used to discuss the lattice dynamics. In the simple harmonic oscillator model:

$$\nu = \frac{1}{2\pi c}\sqrt{\frac{k}{\mu}} \quad \text{or} \quad k = 4\pi^2 c^2 \mu \nu^2 \tag{3}$$

where ν is the vibrational frequency of the stretching band, and μ is the reduced mass of the two-mass system. Two X-O stretching bands [$A_g(\nu_1)$ and $E_g(\nu_1)$] exist for each ilmenite type. We calculated *k* from the stretching-band frequencies at each condition and obtained the temperature and pressure derivatives of *k* (Fig. 5; Table 2). For XO_6 octahedra of the ilmenite structure, there were two types of X-O bonds (Fig. 1): longer X-O bonds opposed to the shared face in MO_6 octahedra and shorter X-O bonds opposed to the unshared face. Commonly, for a covalent model such as silicates, germanates, and titanates, a quantitative connection between *k* and the cation-anion bond length, *r*, exists (Batsanov and Derbeneva 1969; Hofmeister 1993):

$$k \propto \left(\frac{e_+ e_-}{r^2}\right)^{\frac{3}{4}} \tag{4}$$

where *e* is the electronegativity of each of the two ions. Since $A_g(\nu_1)$ had a higher frequency and a larger *k* value than $E_g(\nu_1)$, $A_g(\nu_1)$ corresponded to the stretching band for shorter X-O bonds (unshared face), and $E_g(\nu_1)$ was the stretching band for longer X-O bonds (shared face), to a first approximation.

Table 2 shows the temperature derivatives of *k* of both $A_g(\nu_1)$ and $E_g(\nu_1)$ of the three ilmenite types. Generally, for the bond that has high absolute $\delta k/\delta T$, the rate of change of the interatomic bonding force with temperature is high, i.e., the rate at which the bond length becomes long is high. We noticed the magnitude relations between the absolute $\delta k/\delta T$ of $A_g(\nu_1)$ and that of $E_g(\nu_1)$ in the isochemical ilmenites are as follows. For Si-O and Ge-O bonds, the absolute $\delta k/\delta T$ of $A_g(\nu_1)$ are higher than that of $E_g(\nu_1)$. Namely, shorter Si-O or Ge-O bonds [$A_g(\nu_1)$, unshared face] were more lengthened with temperature than the longer Si-O or Ge-O bonds [$E_g(\nu_1)$, shared face]. Therefore, the cation positions moved along the direction of the **c** axis with temperature and tended to approach the center of the SiO_6 or GeO_6 octahedra with increasing temperature. This phenomenon indicates that the length of the shorter Si-O or Ge-O bonds [$A_g(\nu_1)$, unshared face] becomes equal to that of the longer Si-O or Ge-O bonds [$E_g(\nu_1)$, shared face] by thermal expansion, and the regularity of SiO_6 or GeO_6 octahedra is enhanced at high temperatures. In contrast, for Ti-O bonds, the absolute $\delta k/\delta T$ of $A_g(\nu_1)$ was smaller than that of $E_g(\nu_1)$—the longer Ti-O bonds [$E_g(\nu_1)$, shared face] were more lengthened with temperature than were the shorter Ti-O bonds [$A_g(\nu_1)$, unshared face]. Therefore, the Ti positions moved along the direction of the **c** axis away from the center with increasing temperature, indicating that the distortion of the TiO_6 octahedra is enhanced at high temperatures. In previous reports, high-temperature Raman spectra of $MgSiO_3$- and $MgTiO_3$-type

TABLE 1. Vibrational mode assignment, frequencies under ambient conditions, and temperature and pressure derivatives of the frequencies of ilmenite types $MgSiO_3$, $MgGeO_3$, and $MgTiO_3$

Mode	Assignment	ν_i (cm^{-1})			$-(\delta\nu_i/\delta T)_P$ (cm^{-1}/K)			$(\delta\nu_i/\delta P)_T$ (cm^{-1}/GPa)		
		$MgSiO_3$	$MgGeO_3$	$MgTiO_3$	$MgSiO_3$	$MgGeO_3$	$MgTiO_3$	$MgSiO_3$	$MgGeO_3$	$MgTiO_3$
$E_g(\nu_5)$	T(Mg)	291	203	224	0.013	0.016	0.023		1.080	0.966
$A_g(\nu_5)$	T(Mg)	352		281	0.012		0.017			1.172
$E_g(\nu_4)$	T(XO_6)		314	306		0.015	0.017		2.028	1.368
$A_g(\nu_4)$	T(XO_6)	412	330	327	0.021	0.011	0.010	2.068	1.208	1.503
$A_g(\nu_3)$	O-X-O bend	481	377	352	0.028	0.017	0.021	2.822	2.213	2.513
$E_g(\nu_3)$	O-X-O bend			397			0.011			2.957
$E_g(\nu_2)$	O-X-O bend		451	485		0.011			2.909	3.218
$A_g(\nu_2)$	O-X-O bend	622	474	487	0.018	0.026	0.026	3.268	3.300	4.143
$E_g(\nu_1)$	X-O stretch	687	615	641	0.016	0.021	0.011	3.413	3.370	4.345
$A_g(\nu_1)$	X-O stretch	802	719	714	0.016	0.021	0.010	3.825	3.909	3.429

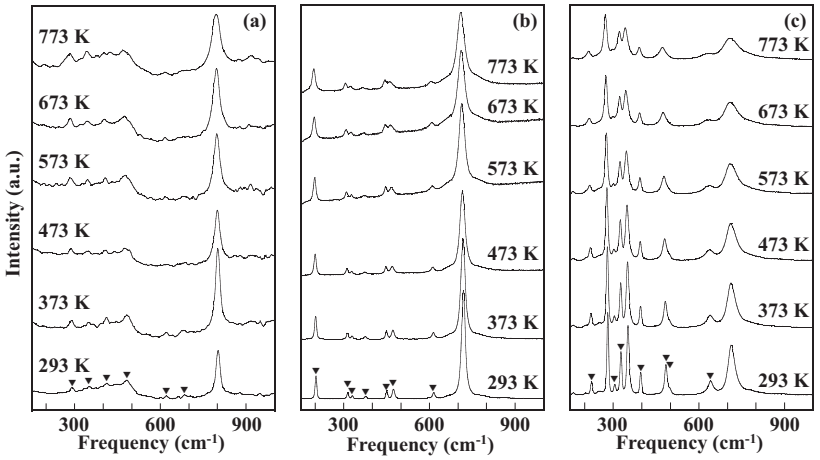

FIGURE 2. Temperature dependence of the Raman spectra of ilmenite types (**a**) $MgSiO_3$, (**b**) $MgGeO_3$, and (**c**) $MgTiO_3$.

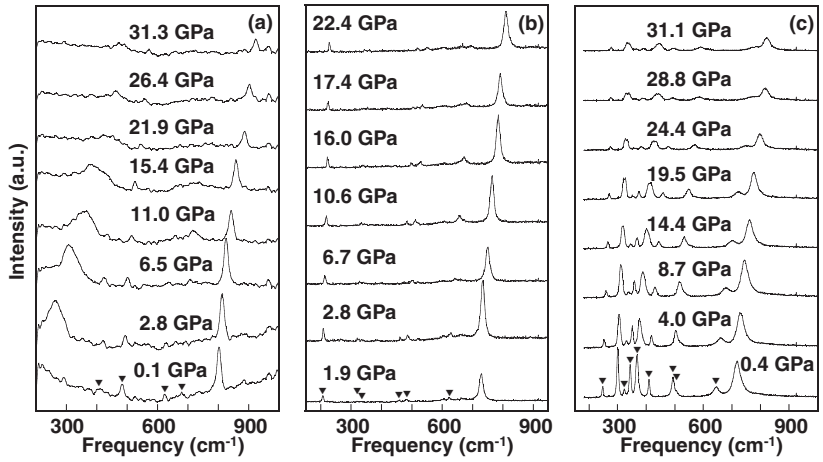

FIGURE 3. Pressure dependence of the Raman spectra of ilmenite types (**a**) $MgSiO_3$, (**b**) $MgGeO_3$, and (**c**) $MgTiO_3$.

TABLE 2. Temperature and pressure derivatives of *k*

	$-(\delta k/\delta T)$ (10^{-4} N m^{-1} K^{-1})			$(\delta k/\delta P)$ (10^{-2} N m^{-1} GPa^{-1})		
	$A_g(\nu_1)$		$E_g(\nu_1)$	$A_g(\nu_1)$		$E_g(\nu_1)$
Si-O stretch	136(7)	>	92(50)	397(6)	>	310(10)
Ge-O stretch	209(2)	>	131(9)	468(3)	>	328(19)
Ti-O stretch	81(5)	<	90(9)	374(7)	<	437(8)

ilmenites had been collected up to 1030 and 1820 K at ambient pressure, respectively (Reynard and Rubie 1996; Reynard and Guyot 1994). Although these authors did not calculate the $\delta k/\delta P$ of the stretching bands, we can estimate the strength of $A_g(\nu_1)$ and $E_g(\nu_1)$ against temperature from the magnitude relations between the absolute $\delta\nu/\delta T$ of $A_g(\nu_1)$ and that of $E_g(\nu_1)$ in their experimental results. For $MgSiO_3$-ilmenite, the absolute $\delta\nu/\delta T$ of $A_g(\nu_1)$ (0.0212 cm^{-1}/K) is slightly lower than that of $E_g(\nu_1)$ (0.0245 cm^{-1}/K) (Reynard and Rubie 1996). This is contradictory to our results. For the Si-O bond, the strength of $A_g(\nu_1)$ against temperature might be almost equal to that of $E_g(\nu_1)$. For $MgTiO_3$-ilmenite, that of $A_g(\nu_1)$ (0.0098 cm^{-1}/K) was lower than that of $E_g(\nu_1)$ (0.0217 cm^{-1}/K) (Reynard and Guyot 1994). This is consistent with our results.

For both $A_g(\nu_1)$ and $E_g(\nu_1)$, the magnitude of the absolute $\delta k/\delta T$ of the Ge-O stretching band was the highest, that of Si-O was second, and that of Ti-O was the lowest (Table 2). Since the relation between the interatomic bonding force of a two-dimensional bonding system and the expansion rate of a three-dimensional lattice system is not so simple, the magnitude relation of $\delta k/\delta T$ cannot be equated to that of the XO_6 thermal expansion rate of each ilmenite.

The difference in expansion behavior could depend on whether the ilmenite is thermodynamically stable at ambient pressure and temperature conditions. The $MgTiO_3$-ilmenite is thermodynamically stable at ambient conditions. However, with increasing temperature, the longer Ti-O bonds [$E_g(\nu_1)$, shared face] might lengthen more than the shorter Ti-O bonds [$A_g(\nu_1)$, unshared face] due to the effect of thermal expansion of the MgO_6 octahedra whose volume is much larger than that of TiO_6. On the other hand, $MgSiO_3$- and $MgGeO_3$-ilmenites are metastable at ambient conditions and could expand anisotropically rather than unit-cell volume of those ilmenite in thermodynamically stable state at high pressures. At ambient conditions, the shorter

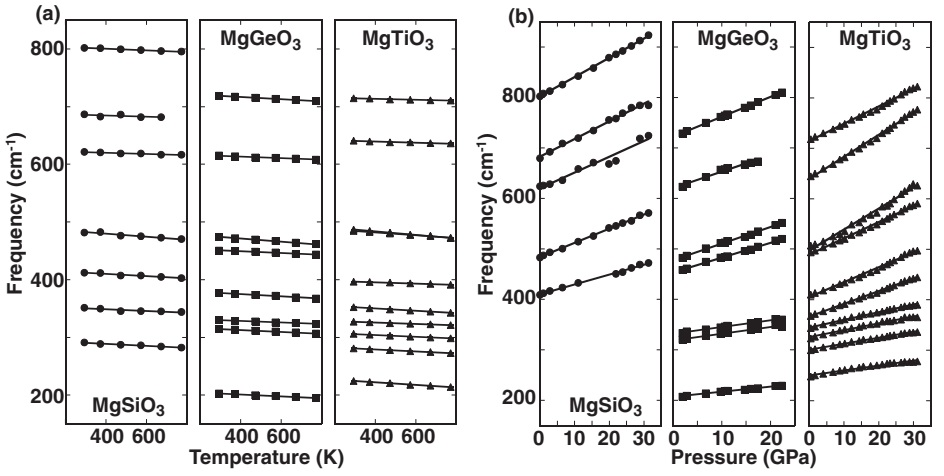

FIGURE 4. Evolution of Raman frequencies of ilmenite types $MgSiO_3$, $MgGeO_3$, and $MgTiO_3$ with (**a**) temperature and (**b**) pressure.

Si-O or Ge-O bonds [$A_g(\nu_1)$, unshared face] could lengthen, since there is vacant space on the opposite side of the unshared face; it should be almost the same length as the longer Si-O or Ge-O bonds [$E_g(\nu_1)$, shared face]. Indeed, in Yamanaka et al. (2005), at ambient conditions, the ratio of the shorter Ti-O bond [$A_g(\nu_1)$] length to the longer Ti-O bond [$E_g(\nu_1)$] length is 0.892. In contrast, (shorter Ge-O)/(longer Ge-O) is 0.952 and (shorter Si-O)/(longer Si-O) is 0.962, both close to 1. These phenomena indicate that although $MgSiO_3$- and $MgGeO_3$-ilmenites maintain those symmetry and fundamental structures as $MgTiO_3$-ilmenite metastably under ambient conditions, they are unquenchable microscopically. In our high-temperature experiments, the length of the shorter Si-O or Ge-O bonds must become more nearly equal to those of the longer Si-O or Ge-O bonds by thermal expansion. Alternatively, we can interpret the different behavior of $MgTiO_3$-ilmenite as due to the fact that Ti is a 3d transition metal unlike Si and Ge.

Table 2 also shows the pressure derivatives of k. The behavior of the $\delta k/\delta P$ should be the inverse of the above-mentioned $\delta k/\delta T$. For the bond that has high absolute $\delta k/\delta P$, the changing rate of interatomic bonding force with pressure is high; the rate at which the bond distance shortens is high. We also noticed the magnitude relations between the absolute $\delta k/\delta P$ of $A_g(\nu_1)$ and that of $E_g(\nu_1)$ in the isochemical ilmenites. For Si-O and Ge-O bonds, the absolute $\delta k/\delta P$ of $A_g(\nu_1)$ were higher than that of $E_g(\nu_1)$: the shorter Si-O or Ge-O bonds [$A_g(\nu_1)$, unshared face] were more shortened with pressure than the longer Si-O or Ge-O bonds [$E_g(\nu_1)$, shared face]. Therefore, the cation positions moved away from the center with increasing pressure, indicating that the distortion of SiO_6 or GeO_6 octahedra is enhanced at high pressures. In contrast, for Ti-O bonds, the absolute $\delta k/\delta P$ of $A_g(\nu_1)$ was smaller than that of $E_g(\nu_1)$: the longer Ti-O bonds [$E_g(\nu_1)$, shared face] were more shortened with pressure than the shorter Ti-O bonds [$A_g(\nu_1)$, unshared face]. Therefore, the Ti positions tended to approach the center of the TiO_6 octahedra with pressure, indicating that the regularity of TiO_6 octahedra is enhanced at high pressures. In previous reports, high-pressure Raman spectra of $MgSiO_3$- and $MgTiO_3$-ilmenites had been collected up to 7 and 27 GPa at room temperature, respectively (Reynard and Rubie 1996; Reynard and Guyot 1994). For the $MgSiO_3$-ilmenite, the absolute $\delta\nu/\delta P$ of $A_g(\nu_1)$ (3.7 $cm^{-1}\cdot GPa^{-1}$) was higher than that of $E_g(\nu_1)$ (3.3 $cm^{-1}\cdot GPa^{-1}$) (Reynard and Rubie 1996). For $MgTiO_3$ ilmenite, that of $A_g(\nu_1)$ (3.10 $cm^{-1}\cdot GPa^{-1}$) was lower than that of $E_g(\nu_1)$ (4.88 $cm^{-1}\cdot GPa^{-1}$) (Reynard and Guyot 1994). Both results were consistent with our results.

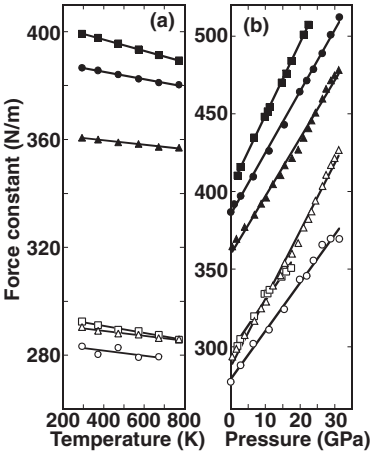

FIGURE 5. Evolution of the force constant, k, with (**a**) temperature and (**b**) pressure. Solid circles represent $A_g(\nu_1)$ of Si-O stretching band; open circles, $E_g(\nu_1)$ of Si-O; solid squares, $A_g(\nu_1)$ of Ge-O; open squares, $E_g(\nu_1)$ of Ge-O; solid triangles, $A_g(\nu_1)$ of Ti-O; and open triangles, $E_g(\nu_1)$ of Ti-O.

The order of magnitude of the absolute $\delta k/\delta P$ of $E_g(\nu_1)$ in the three samples was quite different from that of $A_g(\nu_1)$ as shown in Table 2. The magnitude relation of the X-O interatomic bonding force cannot be compared directly with that of the bulk modulus of each XO_6 octahedron: TiO_6 was the easiest to be compressed (K_{T,TiO_6} = 245 GPa), GeO_6 was second ($K_{T,\ GeO_6}$ = 268 GPa), and SiO_6 was the hardest (K_{T,SiO_6} = 292 GPa) (Yamanaka et al. 2005).

The difference in compression behavior could be explained by evaluating whether the ilmenite is thermodynamically stable

at ambient *P-T* conditions. For a stable $MgTiO_3$-ilmenite at ambient conditions, with increasing pressure, the longer Ti-O bonds [$E_g(\nu_1)$, shared face] might shorten more than the shorter Ti-O bonds [$A_g(\nu_1)$, unshared face] due to the influence of the compression of the MgO_6 octahedra, whose volume is much larger than that of TiO_6. On the other hand, the SiO_6 or GeO_6 octahedra of metastable $MgSiO_3$- and $MgGeO_3$-ilmenites at ambient conditions have almost equal lengths of the Si-O or Ge-O bonds as mentioned above. In our high-pressure experiments, since the metastable ilmenite compounds approach a thermodynamically stable state by compression, the lengthened Si-O or Ge-O bonds [$A_g(\nu_1)$, unshared face] should be shortened, and the SiO_6 or GeO_6 octahedra should return to the stable form with the two-types of Si-O or Ge-O bonds. Alternatively, we can also interpret the different behavior of $MgTiO_3$-ilmenite as due to the fact that Ti is a 3d transition metal.

In the above discussion, we regard the *P-T* dependencies of the Raman frequencies and the force constants of the three ilmenite types to be linear. However, only the pressure dependences of those of $MgTiO_3$-ilmenite, especially $A_g(\nu_1)$ and $E_g(\nu_1)$, seem not to be linear (Figs. 4b and 5). The pressure dependencies seem to have curvatures at about 20 and 25 GPa: the slopes become sharp at 20 GPa and gentle at 25 GPa. It was mentioned above that the magnitude of the absolute $\delta k/\delta P$ of the stretching bands indicates that of the bonding force, i.e., the rate to which the bond length becomes short. Thus, these variations of $\delta k/\delta P$ of $MgTiO_3$-ilmenite should show that the rates to which the Ti-O bonds become shorter change at 20 and 25 GPa. We interpreted these phenomena as follows: the entire TiO_6 octahedra could be compressed comparatively isotropically up to 20 GPa while the Ti positions that approved the center of the TiO_6 octahedra could be much enhanced at 20–25 GPa, and above 25 GPa such movement of Ti could be obstructed due to the repulsion between Ti atoms which share edge. One of the reasons for these curvatures may be the fact that Ti is a 3d transition metal. Supposing this reason is incorrect, also in $MgSiO_3$- and $MgGeO_3$-ilmenites, then these curvatures must occur at higher pressure than our experimental pressure regions. Single-crystal X-ray analyses at higher pressure will solve the reason for these curvatures.

Yamanaka et al. (2005) conducted a single-crystal XRD study under high pressures on of $MgSiO_3$-, $MgGeO_3$-, and $MgTiO_3$-ilmenites and showed a pressure dependence of interatomic distances of the Si-O, Ge-O, and Ti-O bonds up to 10 GPa. In Figure 3 of Yamanaka et al. (2005), it is clear that the longer Ti-O bonds [$E_g(\nu_1)$, shared face] were shortened more than the shorter Ti-O bonds [$A_g(\nu_1)$, unshared face] with increasing pressure. In contrast, the shorter Si-O or Ge-O bonds [$A_g(\nu_1)$, unshared face] were shortened than the longer Si-O or Ge-O bonds [$E_g(\nu_1)$, shared face]. Therefore, the XRD results of Yamanaka et al. (2005) are consistent with our Raman results and discussion. Thus, for the XO_6 octahedra of ilmenite, the general rule—that the large variation of *k* with pressure is attributed to the weakness of the bonding force—stands up. In the virial equation of state (Eq. 1), the pressure provided by the external system, P_{ext}, makes not only the interatomic distances, r_{ij}, to be shortened, and but also the interatomic force, F_{ij}, to be strengthened. The Raman vibrational frequency corresponds to interatomic bonding energy, which leads to interatomic distance. Thus, the Raman spectroscopic studies at high temperatures and high pressures are useful in clarifying the mechanisms of expansion and compression.

For each stretching band of three ilmenites, Figure 6 shows the relation between the force constants, *k*, calculated from the present frequencies using Equation 3 and the $(1/r)^{3/2}$ values of Equation 4 at the identical pressure. The X-O bond lengths, *r*, at each pressure are extrapolated linearly from the relations between *r* and pressure obtained by Yamanaka et al. (2005) up to 10 GPa. The $(1/r)^{3/2}$ values are nearly proportional to *k* values in each mode. This finding demonstrates that Equation 4 is affirmed for the three ilmenite types of the study, even for the longer X-O bonds [$E_g(\nu_1)$, shared face], which are not nearest-neighbor relations. This finding also shows that the simple harmonic oscillator model dominates even the longer, i.e., second neighbor, X-O bonds in the present study.

Anharmonic effect on the thermodynamic properties

From the obtained frequency shifts with temperature and pressure, the isobaric and isothermal mode Grüneisen parameters, γ_{iP} and γ_{iT}, can be calculated as follows (Gillet et al. 1989):

$$\gamma_{iP} = -\left(\frac{\partial \ln \nu_i}{\partial \ln V}\right)_P = -\frac{1}{\alpha}\left(\frac{\partial \ln \nu_i}{\partial T}\right)_P \quad (5)$$

$$\gamma_{iT} = -\left(\frac{\partial \ln \nu_i}{\partial \ln V}\right)_T = K_T\left(\frac{\partial \ln \nu_i}{\partial P}\right)_T \quad (6)$$

where ν_i is the vibrational frequency of the i^{th} band, α is the thermal expansivity, and K_T is the isothermal bulk modulus. Although these formulas are commonly considered to be definitions, averaging γ_{iP} and γ_{iT} values obtained from Equations 5 and 6 typically underestimates the thermal Grüneisen parameter, $\gamma_{th} = \alpha K_T V/C_V$ [e.g., Chopelas et al. 1994 (for γ-Mg_2SiO_4)]. Hofmeister and Mao (2002) realized that the discrepancies arise because Equations 5 and 6 do not account for differential expansion and

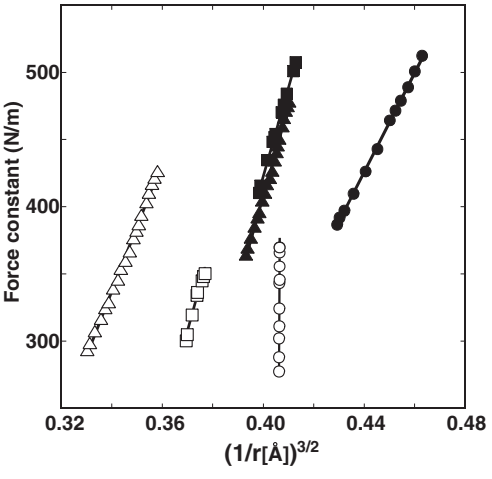

FIGURE 6. Relation between the force constants calculated from the present frequencies using Equation 3 and the $(1/r)^{3/2}$ values of Equation 4 at the identical pressure. The X-O bond lengths, *r*, at each pressure are extrapolated linearly from the relations between *r* and pressure obtained by Yamanaka et al. (2006) up to 10 GPa. Symbols are as in Figure 5.

compression in structures with functional groups and proposed that for each vibration in a solid, γ_{iP} and γ_{iT} should be computed by using the volume that changes during the particular atomic motion correlated with each given frequency as follows:

$$\gamma_{iP}^{*} = -\left(\frac{\partial \ln \nu_i}{\partial \ln V_a}\right)_P = -\frac{1}{\alpha_a}\left(\frac{\partial \ln \nu_i}{\partial T}\right)_P \quad (7)$$

$$\gamma_{iT}^{*} = -\left(\frac{\partial \ln \nu_i}{\partial \ln V_a}\right)_T = K_{Ta}\left(\frac{\partial \ln \nu_i}{\partial P}\right)_T \quad (8)$$

where α_a is the thermal expansivity and K_{Ta} is the bulk modulus associated with the volume vibrating (V_a). For many of the optical modes in polyatomic structures such as ilmenite, α_a and K_{Ta} will be a polyhedral thermal expansivity, $[\delta V_a/\delta T]/V_a$, and a polyhedral bulk modulus, $-V_a/[\delta V_a/\delta P]$, respectively, but for optical modes involving complex motions of all atoms, α and K_T pertain. Thus, application of Equations 7 and 8 requires band assignments and the relevant polyhedron is deduced from the band assignments. The comparatively low frequency modes [$E_g(\nu_5)$, $A_g(\nu_5)$, $E_g(\nu_4)$, and $A_g(\nu_4)$] are assigned to translations of Mg^{2+} cation against O, or of the XO_6 octahedra moving as a unit against Mg^{2+}. Because all of these motions involve the Mg^{2+} cation against O atoms, α_a and K_{Ta} are the polyhedral thermal expansivity and bulk modulus of the MgO_6 octahedron, respectively. The symmetric O-X^{4+}-O bends [$E_g(\nu_3)$, $A_g(\nu_3)$, $E_g(\nu_2)$, and $A_g(\nu_2)$] active in Raman spectra, which are simple expansion and compression of the XO_6 octahedron, must involve compression and expansion of the adjacent MgO_6 octahedron; therefore, $\alpha_a = \alpha$ and $K_{Ta} = K_T$. The X^{4+}-O stretches [$E_g(\nu_1)$ and $A_g(\nu_1)$], which are motions of X^{4+} against O, need not involve the adjacent Mg^{2+} cation; hence, α_a and K_{Ta} is the polyhedral thermal expansivity and bulk modulus of XO_6 octahedron, respectively. We used $\alpha = 2.44 \times 10^{-5}$ K^{-1} (Ashida et al. 1988), $K_T = 219$ GPa, $K_{T,MgO_6} = 172$ GPa, and $K_{T,SiO_6} = 292$ GPa (Yamanaka et al. 2005) for $MgSiO_3$, $\alpha = 2.24 \times 10^{-5}$ K^{-1} (Ashida et al. 1985), $K_T = 180$ GPa, $K_{T,MgO_6} = 139$ GPa, and $K_{T,GeO_6} = 268$ GPa (Yamanaka et al. 2005) for $MgGeO_3$, and $\alpha = 3.01 \times 10^{-5}$ K^{-1}, $\alpha_{MgO_6} = 3.74 \times 10^{-5}$ K^{-1}, and $\alpha_{TiO_6} = 2.45 \times 10^{-5}$ K^{-1} (estimated from values of $FeTiO_3$; Wechsler and Prewitt 1984) and $K_T = 161$ GPa, $K_{T,MgO_6} = 116$ GPa, and $K_{T,TiO_6} = 245$ GPa (Yamanaka et al. 2005) for $MgTiO_3$. Since the polyhedral thermal expansivities of $MgSiO_3$ and $MgGeO_3$ are unavailable, we cannot calculate γ_{iP}^{*} of those ilmenite types. The values of γ_{iP}, γ_{iT}, γ_{iP}^{*}, and γ_{iT}^{*} calculated for each vibrational band are reported in Table 3. Each average $\langle\gamma_{iT}\rangle$ value is slightly lower than each average $\langle\gamma_{iT}^{*}\rangle$. These results correspond with that averaging γ_{iT} values underestimate the thermal Grüneisen parameter, $\gamma_{th} = \alpha K_T V/C_V$ (e.g., Chopelas et al. 1994). However, the average $\langle\gamma_{iP}\rangle$ of $MgTiO_3$ is higher than the average $\langle\gamma_{iP}^{*}\rangle$. The difference might be caused by the that the polyhedral thermal expansivities of $FeTiO_3$ were used for those of $MgTiO_3$-ilmenite. In Reynard and Rubie (1996) for $MgSiO_3$-ilmenite, the values of γ_{iP} are scattered between 1.05 and 2.3 ($\langle\gamma_{iP}\rangle = 1.60$) and those of γ_{iT} between 0.88 and 1.6 ($\langle\gamma_{iT}\rangle = 1.21$). In Reynard and Guyot (1994) for $MgTiO_3$-ilmenite, the values of γ_{iP} are scattered between 0.5 and 3.2 ($\langle\gamma_{iP}\rangle = 1.41$) and those of γ_{iT} between 0.7 and 1.35 ($\langle\gamma_{iT}\rangle = 1.10$). The degree and range of scattering of the Grüneisen parameters in the present study were not significantly different from those reported in previous studies.

The intrinsic anharmonic mode parameter, a_i, also can be estimated using the values of the γ_{iP} and γ_{iT} as follows (Gillet et al. 1989):

$$a_i = \left(\frac{\partial \ln \nu_i}{\partial T}\right)_V = \alpha K_T\left(\frac{\partial \ln \nu_i}{\partial P}\right)_T - \left(\frac{\partial \ln \nu_i}{\partial T}\right)_P = \alpha\left(\gamma_{iT} - \gamma_{iP}\right) \quad (9)$$

Correctly, a_i should be estimated using γ_{iP}^{*} and γ_{iT}^{*}. However, since γ_{iP}^{*} and a_i^{*} can be calculated only for $MgTiO_3$-type ilmenite, we adopt a_i calculated using γ_{iP} and γ_{iT} in the present discussion. The values of calculated α_i and a_i^{*} of each vibrational band are reported in Table 3, and α_i of three ilmenite types are plotted in Figure 7. The values for the high-frequency bands were not significantly different from zero (the vertical axis $\alpha = 0$ in Fig. 7). However, the α_i for the low-frequency bands were negative numbers, and the absolute values were relatively large. The frequency of the external modes (translation bands of XO_6 or Mg cation) was lower than that of the internal modes of XO_6 octahedra (X-O stretching bands or O-X-O bending bands)—i.e., the bonding force of the external modes was weaker than that of the internal modes. Thus, the external modes have higher absolute values of α_i and are influenced by the anharmonicity more easily than the internal modes.

All models of thermodynamic properties are quasi-harmonic and based on a partition function that assumes frequencies are independent of temperature. However, Gillet et al. (1991) tried to quantify anharmonicity by relaxing the quasi-harmonic assumption $(\delta \ln \nu_i/\delta T)_V = 0$. With the anharmonic contribution, the isochoric specific heat, C_V, is expressed as follows (Gillet et al. 1991):

$$C_V = 3nR\sum_{i=1}^{m} C_{Vi}^{\,h}\left(1 - 2a_i T\right) \quad (10)$$

where n is the number of atoms in the mineral formula, R is the gas constant, and C_{Vi}^{h} is the harmonic part of the isochoric specific heat of the i^{th} mode. The anharmonic correction term on

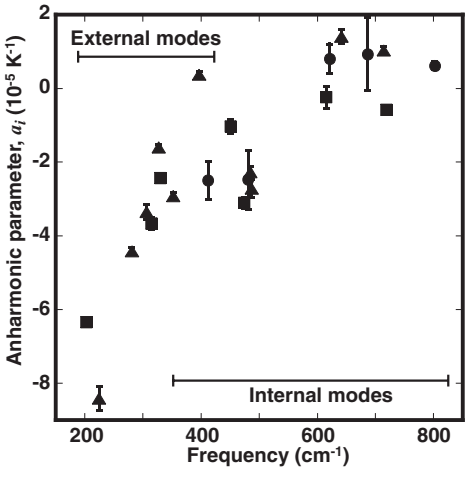

FIGURE 7. Calculated anharmonic mode parameters, a_i, of each vibrational band against Raman frequencies of each band under ambient condition. Solid circles represent $MgSiO_3$; solid squares, $MgGeO_3$; solid triangles, $MgTiO_3$.

TABLE 3. The values of calculated γ_{iP}, γ^*_{iP}, γ_{iT}, γ^*_{iT}, a_i, and a^*_i of each vibrational band

Mode	V_α	$MgSiO_3$				$MgGeO_3$				$MgTiO_3$					
		γ_{iP}	γ_{iT}	γ^*_{iT}	a_i (10^{-5} K^{-1})	γ_{iP}	γ_{iT}	γ^*_{iT}	a_i (10^{-5} K^{-1})	γ_{iP}	γ^*_{iP}	γ_{iT}	γ^*_{iT}	a_i (10^{-5} K^{-1})	a^*_i (10^{-5} K^{-1})
$E_g(\nu_5)$	MgO_6	2.41(15)				3.67(2)	0.84(3)	0.65(2)	−6.34(11)	3.38(8)	2.72(6)	0.59(3)	0.42(2)	−8.41(32)	−8.59(31)
$A_g(\nu_5)$	MgO_6	1.76(42)								2.06(2)	1.66(2)	0.59(1)	0.43(1)	−4.42(9)	−4.60(9)
$E_g(\nu_4)$	MgO_6					2.35(3)	0.71(4)	0.55(3)	−3.67(16)	1.75(5)	1.41(4)	0.64(2)	0.46(1)	−3.35(21)	−3.55(20)
$A_g(\nu_4)$	MgO_6	2.00(19)	0.98(2)	0.77(2)	−2.50(52)	1.77(3)	0.69(3)	0.53(2)	-2.43(12)	1.19(1)	0.96(1)	0.66(1)	0.47(1)	−1.60(8)	−1.81(8)
$A_g(\nu_3)$	$MgXO_3$	2.19(31)	1.17(2)	1.17(2)	−2.48(80)	2.33(13)				1.97(3)	1.97(3)	1.00(1)	1.00(1)	−2.92(10)	−2.92(10)
$E_g(\nu_3)$	$MgXO_3$									0.93(1)	0.93(1)	1.05(1)	1.05(1)	0.37(8)	0.37(8)
$E_g(\nu_2)$	$MgXO_3$					1.55(7)	1.09(2)	1.09(2)	−1.03(19)	1.71(4)	1.71(4)	0.96(1)	0.96(1)	−2.27(15)	−2.27(15)
$A_g(\nu_2)$	$MgXO_3$	0.69(9)	1.02(8)	1.02(8)	0.80(40)	2.53(4)	1.15(3)	1.15(3)	−3.10(15)	2.08(6)	2.08(6)	1.18(2)	1.18(2)	−2.72(24)	−2.72(24)
$E_g(\nu_1)$	XO_6	0.67(37)	1.05(4)	1.39(5)	0.92(99)	1.01(7)	0.91(6)	1.35(9)	−0.24(30)	0.52(5)	0.64(6)	0.99(1)	1.50(1)	1.40(18)	2.11(18)
$A_g(\nu_1)$	XO_6	0.73(4)	0.98(1)	1.31(1)	0.61(11)	1.18(1)	0.92(1)	1.37(2)	−0.58(5)	0.37(2)	0.46(3)	0.72(1)	1.09(1)	1.03(10)	1.55(10)
Average		1.49	1.04	1.13	−0.53	2.05	0.90	0.95	−2.49	1.60	1.45	0.84	0.86	−2.29	−2.25

the specific heat, C'_V, can be expressed with $-6na_iRT$. Since all formulae for C_V were also derived from statistical thermodynamics assuming that frequencies are independent of temperature (Hofmeister 2004), there is a fundamental problem with Equation 10. Moreover, another correction term exists (Wallace 1972) that is negative and of about the same magnitude as $-6na_iRT$ (Hofmeister 2004). Thus, note that the correction term of Gillett et al. (1991), $-6na_iRT$, overestimates the total of the anharmonic correction terms. However, in this study, to discuss the relation between the magnitude of the anharmonic effects and the chemical composition of the ilmenite types, the overestimated $-6na_iRT$ values must be compared. To ensure consistency with the calculation of the harmonic contribution to C_V, the average intrinsic anharmonic mode parameter of α_i in each vibrational band, $\bar{a}$, was used (Table 3). From the obtained $\bar{a}$, the $C'_V \approx -6n\bar{a}RT$ was calculated for each ilmenite types and the relation is shown in terms of temperature in Figure 8. The estimated C'_V were 2.6 J/(mol·K) for $MgSiO_3$, 12.4 J/(mol·K) for $MgGeO_3$, and 11.4 J/(mol·K) for $MgTiO_3$ at 2000 K. In previous studies, the reported C'_V were 4(3) J/(mol·K) for $MgSiO_3$ at 2000 K (Reynard and Rubie 1996) and 3.4 J/(mol·K) for $MgTiO_3$ at 1800 K (Reynard and Guyot 1994). Here, we would like to focus attention on the relation between the magnitude of the anharmonic corrections and the chemical composition of the ilmenite types. The C'_V of $MgGeO_3$ was the highest, $MgTiO_3$ was second, and $MgSiO_3$ was the lowest in the three ilmenites at the same temperature. This descending order of C'_V is different from that of the thermodynamically stable pressure. As shown in Figure 8, the anharmonic effects became larger as temperature became higher. In the quasi-harmonic approximation, the calculated isochoric specific heat tended to approach the classical Dulong-Petit limits ($3n$R) at high temperature, exceeding the Debye temperature. Here, the elastic Debye temperature, Θ_D, can be obtained independently of the frequency as follows (Poirier 1991):

$$\Theta_D = 251.2\left(\frac{\rho}{\overline{M}}\right)^{\frac{1}{3}} \upsilon_m \quad (11)$$

where ρ is a density, $\overline{M}$ is a mean atomic mass, and v_m is a bulk sound velocity calculated from compressional velocity, v_p, and shear velocity, v_s, as follows:

$$v_m = 3^{\frac{1}{3}}\left(\frac{1}{v_p^3}+\frac{2}{v_s^3}\right)^{-\frac{1}{3}} \quad (12)$$

In Poirier (1991), Θ_D = 943 K for $MgSiO_3$-ilmenite was calculated from the reported values of ρ, v_p, and v_s (Weidner and Ito 1985). We also calculated Θ_D = 657 K for $MgGeO_3$ ilmenite and Θ_D = 687 K for $MgTiO_3$-ilmenite from the reported properties (Liebermann 1974, 1976). We can see obviously that the higher the elastic Debye temperature, the smaller the anharmonic effect on C_V.

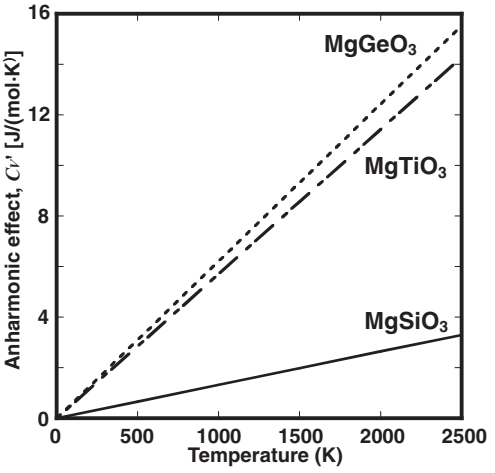

FIGURE 8. Temperature dependence of the calculated Gillet's anharmonic correction term on the isochoric specific heat, $C'_V \approx -6n\bar{a}RT$. Solid line represents $MgSiO_3$; dashed line, $MgGeO_3$; dot-dashed line, $MgTiO_3$.

The present estimation of the anharmonic correction on the specific heat of $MgSiO_3$-ilmenite is very small. Thus, the intrinsic anharmonic corrections to the thermodynamical properties of $MgSiO_3$-ilmenite in the deep interior of the Earth are probably insignificant. Generally, the interatomic potential well becomes deep under high-pressure conditions. The anharmonic effect is not so significant at thermodynamically low temperature, that is, at a much lower temperature than the Debye temperature. However, under such sufficiently high-temperature conditions as exist in the deep mantle of the Earth, a mineral, whose anharmonic effect cannot be ignored, should exist. It is important to clarify the anharmonic effect of various mantle minerals using the method of the present study.

ACKNOWLEDGMENTS

We thank E. Ito and O. Ohtaka for help in synthesizing $MgSiO_3$- and $MgGeO_3$-ilmenite using multi-anvil apparatuses. Critical reviews by three referees (B. Kolesov, A.N. Hofmeister, and L. Dubrovinsky) were helpful in improving the manuscript. This study was supported by the Grant-in-Aid for Scientific Research (No. 14204053) to T.Y. from the Japan Society for the Promotion of Science and

the Grant-in-Aid for the 21st Century Center of Excellence (COE) Program on "Toward a New Basic Science; Depth and Synthesis" (Program Leader: Y. Onuki) at Osaka University to T.O. financed by the Ministry of Education, Culture, Sports, Science and Technology, Japan.

REFERENCES CITED

Ashida, T., Miyamoto, Y., and Kume, S. (1985) Heat capacity, compressibility and thermal expansion coefficient of ilmenite-type $MgGeO_3$. Physics and Chemistry of Minerals, 12, 129–131.

Ashida, T., Kume, S., Ito, E., and Navrotsky, A. (1988) $MgSiO_3$ ilmenite: Heat capacity, thermal expansivity, and enthalpy of transformation. Physics and Chemistry of Minerals, 16, 239–245.

Batsanov, S.S. and Derbeneva, S.S. (1969) Effect of valency and coordination of atoms on position and form of infrared absorption bands in inorganic compounds. Journal of Structural Chemistry, 10, 510–515.

Chopelas, A. (1999) Estimates of mantle relevant Clapeyron slopes in the $MgSiO_3$ system from high-pressure spectroscopic data. American Mineralogist, 84, 233–244.

Chopelas, A., Boehler, R., and Ko, T. (1994) Thermodynamics and behavior of γ-Mg_2SiO_4 at high pressure: implications for Mg_2SiO_4 phase equilibrium. Physics and Chemistry of Minerals, 21, 351–359.

Deer, W.A. and Zussman, J. (1963) Rock-forming minerals, 5, 30–32. Longmans, Green and Co. Ltd., London, U.K.

Fateley, W.G., McDevitt, N.T., and Benly, F.F. (1971) Infrared and Raman selection rules for lattice vibrations: the correlation method. Applied Spectroscopy, 25, 155–174.

Gillet, P., Guyot, F., and Malezieux, J.M. (1989) High-pressure and high-temperature Raman spectroscopy of Ca_2GeO_4: Some insights on anharmonicity. Physics of the Earth and Planetary Interiors, 58, 141–154.

Gillet, P., Richet, P., Guyot, F., and Fiquet, G. (1991) High-temperature thermodynamic properties of forsterite. Journal of Geophysical Research, 95, 21635–21655.

Hofmeister, A.M. (1993) IR reflectance spectra of natural ilmenite: comparison with isostructural compounds and calculation of thermodynamic properties. European Journal of Mineralogy, 5, 281–295.

——— (2004) Thermal conductivity and thermodynamic properties from infrared spectroscopy. In P. King, M. Ramsey, and G. Swayze, Eds., Infrared Spectroscopy in Geochemistry, Exploration Geochemistry, and Remote Sensing, 33, p. 135–154. Mineralogical Association of Canada, Short course series, Québec, Canada.

Hofmeister, A.M. and Mao, H.K. (2002) Redefinition of the mode Grüneisen parameter for polyatomic substances and thermodynamic implications. Proceedings of the National Academy of Sciences, 99, 559–564.

Horiuchi, H., Hirano, M., Ito, E., and Matsui, Y. (1982) $MgSiO_3$ (ilmenite-type): Single crystal X-ray diffraction study. American Mineralogist, 67, 788–793.

Karki, B.B., Duan, W., Da Silva, C.R.S., and Wentzcovitch, R.M. (2000) Ab initio structure of $MgSiO_3$ ilmenite at high pressure. American Mineralogist, 85, 317–320.

Liebermann, R.C. (1974) Elasticity of pyroxene-garnet and pyroxene-ilmenite phase transformations in germanates. Physics of the Earth and Planetary Interiors, 8, 361–374.

——— (1976) Elasticity of ilmenites. Physics of the Earth and Planetary Interiors, 12, 5–10.

Linton, J.A., Fei, Y., and Navrotsky, A. (1999) The $MgTiO_3$-$FeTiO_3$ join at high pressure and temperature. American Mineralogist, 84, 1595–1603.

Mao, H.K., Bell, P.M., Shaner, J.W., and Steinberg, D.J. (1978) Specific volume measurements of Mo, Pd, and Ag and calibration of ruby R1 fluorescence pressure gauge from 0.06 to 1 Mbar. Journal of Applied Physics, 49, 3276–3283.

Matsui, M., Akaogi, M., and Matsumoto, T. (1987) Computational model of the structural and elastic properties of the ilmenite and perovskite phase of $MgSiO_3$. Physics and Chemistry of Minerals, 14, 101–106.

McMillan, P.F. and Ross, N.L. (1987) Heat capacity calculations for Al_2O_3 corundum and $MgSiO_3$ ilmenite. Physics and Chemistry of Minerals, 16, 225–234.

Poirier, J.P. (1991) Introduction to the physics of the Earth's Interior. Cambridge University Press, U.K.

Reynard, B. and Guyot, F. (1994) High-temperature properties of geikielite ($MgTiO_3$-ilmenite) from high-temperature high-pressure Raman spectroscopy—some implications for $MgSiO_3$-ilmenite. Physics and Chemistry of Minerals, 21, 441–450.

Reynard, B. and Rubie, D.C. (1996) High-pressure, high-temperature Raman spectroscopic study of ilmenite-type $MgSiO_3$. American Mineralogist, 81, 1092–1096.

Reynard, B., Fiquet, G., Itie, J-P., and Rubie, D.C. (1996) High-pressure X-ray diffraction study and equation of $MgSiO_3$ ilmenite. American Mineralogist, 81, 45–50.

Ross, N.L. and McMillan, P. (1984) The Raman spectrum of $MgSiO_3$ ilmenite. American Mineralogist, 69, 719–721.

Ross, N.L. and Navrotsky, A. (1988) Study of the $MgGeO_3$ polymorphs (orthopyroxene, clinopyroxene and ilmenite structures) by calorimetry, spectroscopy and phase equilibria. American Mineralogist, 97, 1355–1365.

Sawamoto, H. (1987) Phase diagram of $MgSiO_3$ at pressure up to 24 GPa and temperatures up to 2200 °C: phase stability and properties of tetragonal garnet. In M.H. Manghnani and Y. Syono, Eds., High-pressure in Mineral Physics, p. 209–219. Terra Scientific, Tokyo, Japan.

Tomioka, N. and Fujino, K. (1997) Natural (Mg, Fe)SiO_3-ilmenite and perovskite in the Tenham Meteorite. Science, 277, 352–355.

Wallace, D.C. (1972) Themodynamics of Crystals (sections 16 and 20). John Wiley and Sons, New York.

Wechsler, B.A. and Prewitt, C.T. (1984) Crystal structure of ilmenite ($FeTiO_3$) at high temperature and at high pressure. American Mineralogist, 69, 176–185.

Weidner, D.J. and Ito, E. (1985) Elasticity of $MgSiO_3$ in the ilmenite phase. Physics of the Earth and Planetary Interiors, 40, 65–70.

White, W.B. (1974) Order-disorder effects. In V.C. Farmer, Ed., The Infrared Spectra of Minerals, p. 87–91. Mineralogical Society, London, U.K.

Yamanaka, T., Komatsu, Y., Sugahara, M., and Nagai, T. (2005) Structure change of $MgSiO_3$, $MgGeO_3$ and $MgTiO_3$, ilmenites under compression. American Mineralogist, 90, 1301–1307.

MANUSCRIPT RECEIVED OCTOBER 2, 2006
MANUSCRIPT ACCEPTED JULY 21, 2007
MANUSCRIPT HANDLED BY BRIGITTE WOPENKA